

# A Feasible Way to Find Above-Room-Temperature Ferromagnetic Spintronic Materials: from Flat Band Engineering

Yuanji Xu,<sup>1,\*</sup> Xintao Jin,<sup>1</sup> Jiacheng Xiang,<sup>1</sup> Huiyuan Zhang,<sup>1</sup> and Fuyang Tian<sup>1,†</sup>

<sup>1</sup>*Institute for Applied Physics, University of Science and Technology Beijing, Beijing 100083, China*

(Dated: July 23, 2024)

Finding and designing ferromagnets that operate above room temperature is crucial in advancing high-performance spintronic devices. The pioneering van der Waals (vdW) ferromagnet  $\text{Fe}_3\text{GaTe}_2$  has extended the way for spintronic applications by achieving a record-high Curie temperature among its analogues. However, the physical mechanism of increasing Curie temperature still needs to be explored. Here, we propose a practical approach to discovering high-temperature ferromagnetic materials for spintronic applications through flat band engineering. We simulate the magnetic transition directly from strongly correlated calculations, reconciling the dual nature of  $d$ -electrons with both localization and itinerant characters. Significantly, our systematic studies unveil the emergence of quasi-particle flat bands arising from collective many-body excitations preceding the ferromagnetic phase transition, reinforcing magnetic stability through a positive feedback mechanism. This research provides a promising pathway for exploring next-generation spintronic devices utilizing low-dimensional vdW flat band systems.

**KEYWORDS:** van der Waals ferromagnet, spintronics, flat band, electronic structures, dynamical mean-field theory

Two-dimensional (2D) quantum magnetic systems represent an excellent platform for spintronic applications due to their enhanced scalability, effective gate-voltage control of the band structure, and intriguing magnetic properties.[1–6] Particularly noteworthy is the recently discovered itinerant vdW ferromagnet  $\text{Fe}_3\text{GaTe}_2$ , which exhibits a remarkable ferromagnetic phase transition temperature exceeding 350 K, positioning 2D vdW materials as promising candidates for advancing spintronic technologies.[7] Notably,  $\text{Fe}_3\text{GaTe}_2$  not only boasts a significantly higher Curie temperature ( $T_C$ ) compared to its counterpart  $\text{Fe}_3\text{GeTe}_2$ ,[8, 9] but also demonstrates robust perpendicular magnetic anisotropy (PMA).[9–11] Despite these advancements, the underlying physical mechanisms driving the high- $T_C$  behavior remain incompletely understood. Recent theoretical investigations have made strides in elucidating the origin of this phenomenon, estimating exchange interactions through density functional theory (DFT) calculations combined with a Heisenberg-type Hamiltonian approach.[13–15] These studies reveal that the magnetic interactions in  $\text{Fe}_3\text{GaTe}_2$  and  $\text{Fe}_3\text{GeTe}_2$  are quite intricate, with in-plane couplings playing a pivotal role in differentiating their  $T_C$ . [15]

However, addressing magnetism in itinerant ferromagnets has historically posed challenges due to the dual nature of  $d$ -electrons, which exhibit both localized and itinerant characteristics.[16–19] Experimental and theoretical studies have underscored the critical role of strongly correlated effects in understanding magnetic transitions in 2D vdW ferromagnets.[20–23] For instance, previous experiments have observed significant electron mass enhancement in  $\text{Fe}_3\text{GeTe}_2$ ,[20–22, 24] which shares the same crystal structure as  $\text{Fe}_3\text{GaTe}_2$  shown in Figure 1a. Additionally, angle-resolved photoemission spectroscopy (ARPES) experiments have re-

vealed weak temperature-dependent shifts in bands, indicating that neither the Heisenberg localized model nor the Stoner itinerant model alone can adequately describe itinerant ferromagnets.[25, 26] Recently, Xu and Tian proposed the dynamical correlated model,[27] which accurately accounts for the magnetic phase transition through the spectral weight transfer process, as depicted in Figure 1b. Their theoretical investigation of  $\text{Fe}_3\text{GaTe}_2$  has revealed the emergence of flat bands near the Fermi level. While the strongly correlated community has recently proposed flat band engineering,[28, 29] it is recognized to exert a significant influence on magnetism, heavy fermions, superconductivity, and topology.[30] This perspective suggests a novel approach to exploring high- $T_C$  candidate ferromagnetic spintronic materials based on flat band systems.

In this study, we simulate the magnetic phase transition of vdW ferromagnetic metal  $\text{Fe}_3\text{GaTe}_2$  directly using density functional theory combined with dynamical mean-field theory (DFT+DMFT).[31, 32] Our calculations reveal that magnetic transition occurs above room temperature. Importantly, our simulations circumvent the controversy associated with using the local Heisenberg model to estimate the Curie temperature from the calculated magnetic interactions in itinerant systems. Additionally, our calculations exhibit Curie-Weiss behavior, which can not be captured by the Stoner model.[33] We also observe spectral weight transfer in  $\text{Fe}_3\text{GaTe}_2$ , highlighting the crucial role of correlated effects. Our results demonstrate the emergence of flat bands as temperatures decrease, closely linked to the ferromagnetic phase transition. Furthermore, these flat bands exhibit heavy fermion characteristics at low temperatures and provide positive feedback near the magnetic phase transition at intermediate temperatures, thereby enhancing

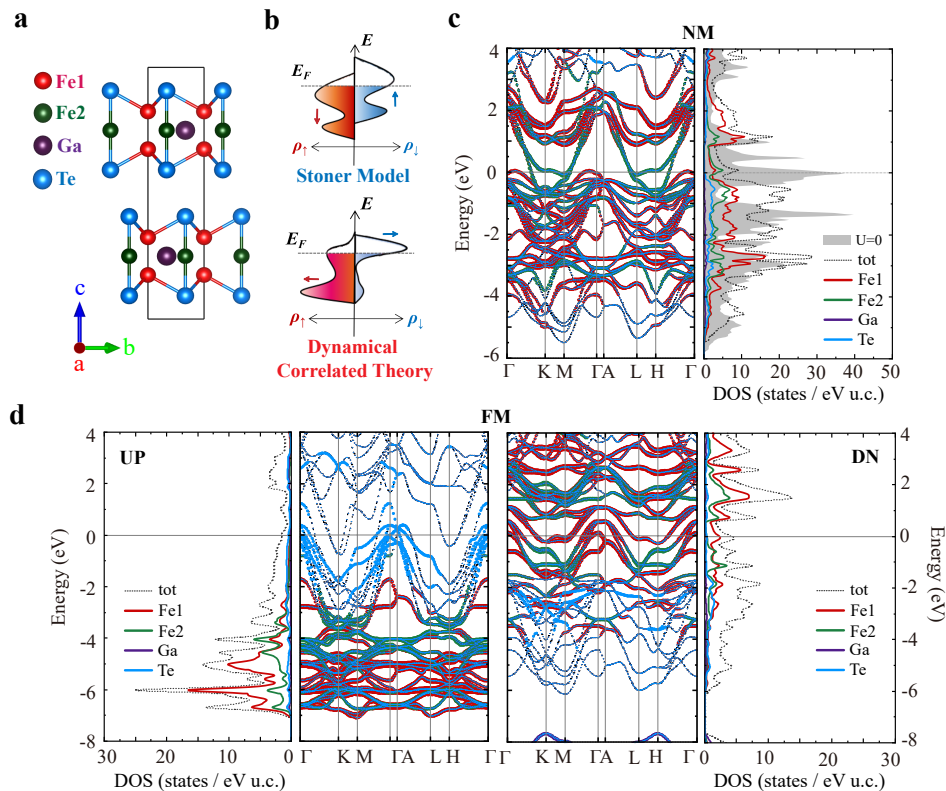


FIG. 1. Crystal structure and electronic structures of  $\text{Fe}_3\text{GaTe}_2$ . (a) Illustration of the crystal structure of  $\text{Fe}_3\text{GaTe}_2$ . (b) Recently proposed paradigm depicting changes in the density of states during magnetic transition in correlated itinerant ferromagnets, considering dynamical correlated effects.[27] (c) Electronic structures and partial density of states from non-spin-polarized calculations of  $\text{Fe}_3\text{GaTe}_2$  in DFT+U calculations. The gray area corresponds to pure DFT calculations. (d) Electronic structures and partial density of states of ferromagnetic order in DFT+U calculations.

the ferromagnetic order. Our findings offer a practical pathway for exploring potential applicable spintronic devices based on 2D vdW flat band systems.

$\text{Fe}_3\text{GaTe}_2$  is a layered vdW ferromagnet featuring two inequivalent Fe sites, designated as Fe1 and Fe2, as depicted in Figure 1a. The central Fe2-Ga layer is nestled between two Fe1 atomic layers, which are further sandwiched by two layers of Te atoms, with a vdW gap between adjacent Te layers.[7] To investigate the origin of high- $T_C$  in  $\text{Fe}_3\text{GaTe}_2$ , the Stoner model, commonly used in itinerant systems, is employed.[24] According to the Stoner model, the high density of states (DOS) at the Fermi level typically satisfies the Stoner criterion, leading to the formation of ferromagnetic order. To elucidate the electronic structures, we performed DFT calculations in both non-magnetic (NM) and spin-polarized ferromagnetic (FM) states. Additionally, we conducted DFT+U calculations to account for strongly correlated effects. Figure 1c compares the electronic structures obtained from DFT and DFT+U calculations. Although the DFT results (represented by the gray area) indicate a considerable DOS at the Fermi level, aligning well with the Stoner picture, the DFT+U calculations reveal a sig-

nificantly reduced DOS at the Fermi level. Similarly, as shown in Figure 1d, the DOS in the ferromagnetic order of DFT+U calculations also exhibits a low value at the Fermi level, which contradicts the expectation of ferromagnetic long-range order based on the Stoner criterion.[33] Furthermore, both experimental and theoretical results indicate that strongly correlated effects are crucial for this type materials.[20-23, 27] What is more, neither DFT nor DFT+U calculations adequately explain the weak temperature-dependent shift of bands within the framework of the Stoner model.[25, 26] These discrepancies highlight the need to reconsider the reliability of conventional DFT-based methods for identifying high- $T_C$  candidate ferromagnetic spintronic materials.

To simulate the magnetic phase transition directly, we further performed magnetic DFT+DMFT calculations, which have yielded reliable results consistent with experimental findings in its sister system,  $\text{Fe}_3\text{GeTe}_2$ . [27, 34, 35] Figure 2 illustrates the evolution of electronic structures as a function of temperature in our DFT+DMFT calculations. At high temperatures, such as 1000 K, the electronic structures of the spin-up and spin-down channels are identical, and the system converges to the NM state.

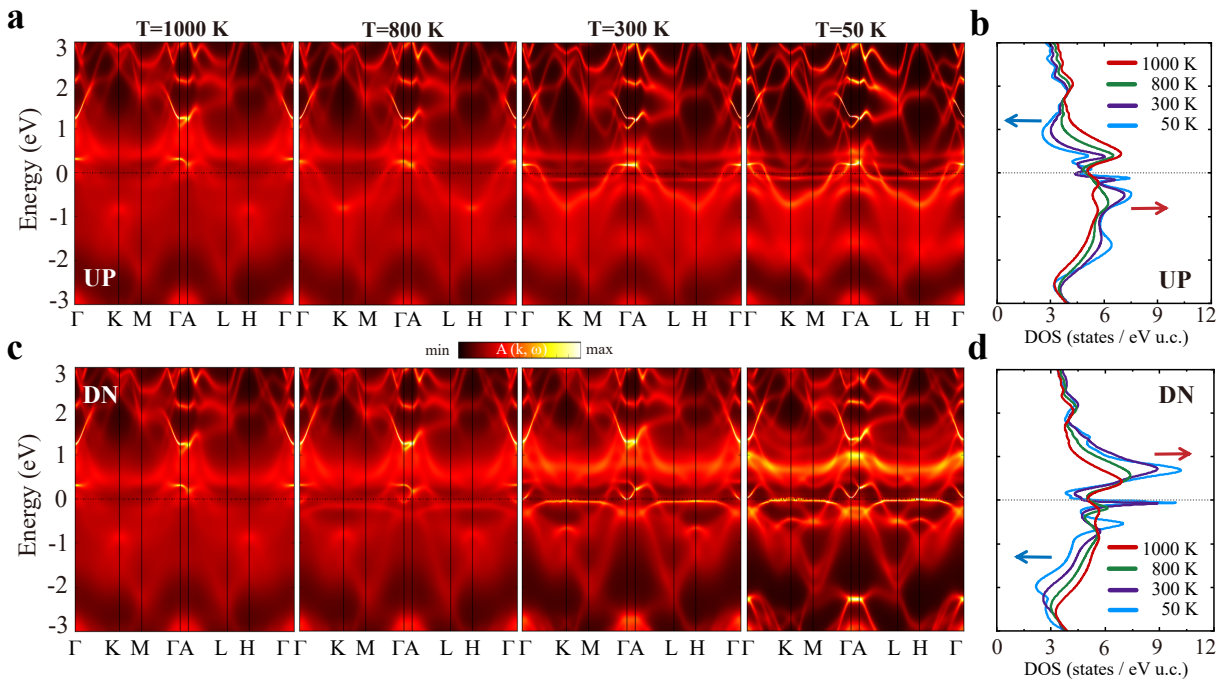


FIG. 2. The DFT+DMFT results of  $\text{Fe}_3\text{GaTe}_2$  with varying temperatures. The calculated spectral functions of the spin-up (a) and spin-down (c) channels are shown for temperatures ranging from 1000 K to 50 K. The corresponding density of states of the spin-up (b) and spin-down (d) channels are also shown for temperatures ranging from 1000 K to 50 K. Blue arrows indicate areas where the density of states decreases with decreasing temperature, while red arrows indicate areas where the density of states increases with decreasing temperature.

The overall DOS at high temperatures is broad, accompanied by large blurred regions in the spectral function. These incoherent characteristics originate from significant spin fluctuations of Fe- $d$  electrons due to strongly correlated effects. Notably, the system undergoes spontaneous symmetry breaking of magnetism at low temperatures, converging to the FM order in our calculations. As shown in Figure 2a and c, the spectral functions of the spin-up and spin-down channels exhibit distinct differences around 300 K. Correspondingly, the DOS in Figure 2b and d shows spectral weight transfer in different tendencies. Specifically, the spectral weight above the Fermi level in the spin-up channel decreases as temperature decreases, while it increases below the Fermi level as temperature decreases. Conversely, the situation is the opposite in the spin-down channel.

In a recent DFT+DMFT study of its sister material,  $\text{Fe}_3\text{GeTe}_2$ , the dynamical correlated effects have been shown to be crucial for accurately capturing the electronic structures.[27] Similarly, the spectral weight transfer process resulting from the dynamical correlated effects is also observed in  $\text{Fe}_3\text{GaTe}_2$ , as depicted in Figure 1b. Additionally, from the DOS in Figures 2b and 2d, sharp peaks begin to form near the Fermi level in both spin channels as the temperature decreases to around 300 K. These renormalized quasi-particle flat bands, as shown

in Figures 2a and 2c, result from the collective excitation of interacting electrons.[16, 27, 34] Furthermore, the quasi-particle flat bands become sharper as the temperature decreases from 300 K to 50 K, indicating the presence of well-defined quasi-particles at low temperatures. Moreover, our calculated electronic structures are in good agreement with recent ARPES measurements.[14, 26] Specifically, there are hole-type bands near the  $\Gamma$  point, electron-type bands near the  $K$  point, lambda-shaped dispersive bands around the  $\Gamma$  and  $A$  points, and low-dispersive bands extending around -0.4 eV. Compared to previous calculations for  $\text{Fe}_3\text{GeTe}_2$ ,[27] the flat bands in  $\text{Fe}_3\text{GaTe}_2$  are much closer to the Fermi level and become flatter. Notably, the flat bands appear disconnected along the  $\Gamma$ - $A$  path near the Fermi level. This disconnection strongly indicates the existence of inter-layer coupling, which may also explain the large magnetic anisotropy in  $\text{Fe}_3\text{GaTe}_2$ . [7] From the above analysis, it is suggested that the high- $T_C$  and large PMA in  $\text{Fe}_3\text{GaTe}_2$  may be closely related to the flat bands.

To gain a deeper physical understanding of these flat bands, we first investigated the electronic structures at the lowest calculated temperature of 50 K. The partial DOS, as shown in Figures 3a and b, indicates that the flat bands primarily originate from the Fe- $d$  electrons. As depicted in Figures 3c to f, in the spin-up chan-

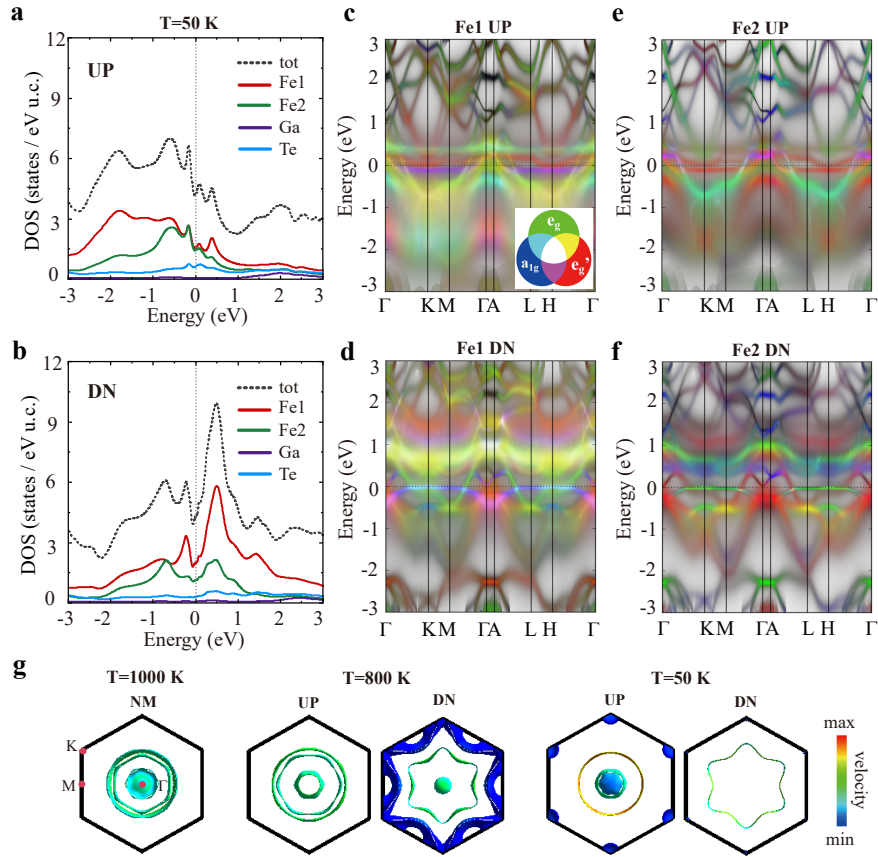


FIG. 3. The partial density of states, spectral function, and Fermi surfaces of  $\text{Fe}_3\text{GaTe}_2$ . (a) Partial density of states at 50 K in the spin-up channel. (b) Partial density of states at 50 K in the spin-down channel. (c) Orbital-resolved spectral function of Fe1 atoms at 50 K in the spin-up channel (c) and in the spin-down channel (d). (e) Orbital-resolved spectral function of Fe2 atoms at 50 K in the spin-up channel (e) and in the spin-down channel (f). (g) Fermi surfaces and their velocity at different temperatures.

nel, the flat bands are located at  $+0.1$  eV and  $-0.15$  eV near the Fermi level. In the spin-down channel, the flat bands are positioned at  $-0.01$  eV, displaying a small peak in the partial DOS in Figure 3b. These renormalized flat bands can be considered heavy quasi-particles that emerge from collective excitations, similar to those found in Hund metals.[16–18] However, in  $\text{Fe}_3\text{GaTe}_2$ , the partial DOS exhibits greater complexity in both spin channels. Additional sharp peaks are observed at  $-0.5$  eV in the spin-up channel and  $-0.2$  eV in the spin-down channel, with contributions from Fe1, Fe2, and Te atoms at almost the same energy positions. These coinciding peak positions suggest hybridization between the localized Fe- $d$  orbitals and other itinerant electrons. Furthermore, the hybridization bands in  $\text{Fe}_3\text{GaTe}_2$  exhibit a complex behavior akin to heavy fermion systems.[36–38] Figures 3c to f illustrate the hybridization characteristics of these flat bands, with the hybridization gap being most pronounced along the  $\Gamma$ -A path. Additionally, as shown in Figure 3g, the Fermi surface velocity decreases at low

temperatures. Consequently, we deduce that  $\text{Fe}_3\text{GaTe}_2$  exhibits heavy fermion behavior at low temperatures, similar to its reported sister material,  $\text{Fe}_3\text{GeTe}_2$ . [21, 22]

We now address the issue of how flat bands improve the magnetic phase transition temperature. The spin susceptibility obtained from NM calculations, as shown in Figure 4a, reveals that Fe1 and Fe2 exhibit Curie-Weiss behavior over a broad temperature range. However, it is noteworthy that the spin susceptibility of Fe2 deviates from the Curie-Weiss law below 400 K. This deviation may arise from the Fe- $d$  electrons forming quasi-particles with screening effects, such as Kondo screening.[39] The enhanced DOS near the Fermi level, derived from DFT+DMFT calculations of the NM state, is significantly larger than that from DFT+U calculations. This increased DOS near the Fermi level enhances the likelihood of a ferromagnetic phase transition.[40] Furthermore, in magnetic DFT+DMFT calculations, as depicted in Figure 4b, the Curie-Weiss law is also observed above Curie temperature. However, there is a

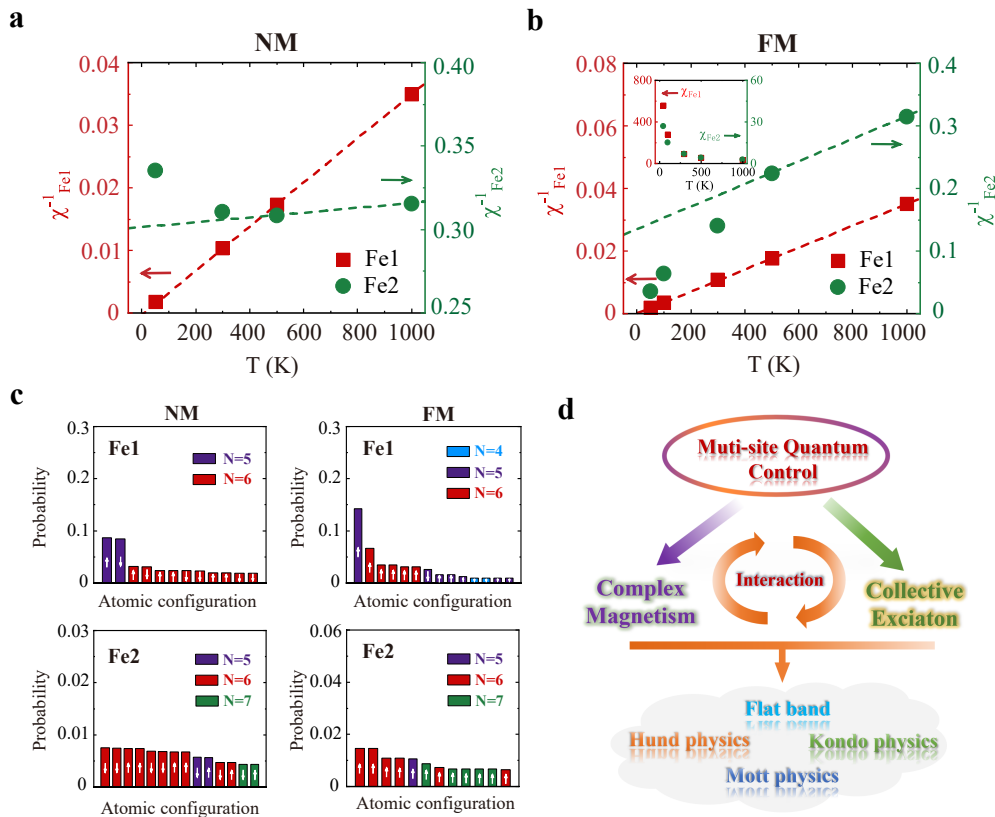


FIG. 4. The discrepancy in the behavior of Fe1 and Fe2 in  $\text{Fe}_3\text{GaTe}_2$ . (a) The inverse spin susceptibility versus temperature in NM calculations. (b) The inverse spin susceptibility versus temperature in FM calculations. (c) The highest probabilities of several Fe atomic states from the impurity solver in the high-temperature NM phase and low-temperature FM phase. (d) A schematic diagram illustrating the interaction of flat bands and magnetism in multi-site correlated itinerant magnets.

notable increase in spin susceptibility (see inset of Figure 4b), and the spin susceptibility of Fe2 deviates from the Curie-Weiss law below the Curie temperature. Notably, while the spin susceptibility of Fe1 is higher than that of Fe2 and increases substantially with decreasing temperature, no deviation from the Curie-Weiss law is observed for Fe1 until the lowest calculated temperature. This suggests that Fe2 may play a crucial role in driving the ferromagnetic transition in  $\text{Fe}_3\text{GaTe}_2$ . The significance of Fe2 is further corroborated by the atomic and orbital-resolved spectral functions shown in Figures 3e and f, which indicate that Fe2 predominantly contributes to the flat bands in both spin channels. Thus, our systematic study first establishes a direct correlation between flat bands and ferromagnetic transition temperature.

The discrepancy between the behavior of Fe1 and Fe2 arises from their distinct local crystal environments.[27] As shown in Fig. 4(c), the highest atomic probabilities from the DMFT impurity solver indicate that Fe1 and Fe2 atoms exhibit significant local moments and considerable spin fluctuations in the high-temperature NM phase. At low temperatures, the highest probabilities for Fe1 and Fe2 are predominantly positive values of  $S_z$ ,

indicating a spontaneous symmetry breaking to ferromagnetic order. Additionally, Fe1 tends to be concentrated in a single charge state, characteristic of Mott-type behavior.[18] In contrast, the histogram for Fe2 spans multiple charge states, indicative of Hundness.[16, 18, 41] This Hundness nature of Fe2 further supports its role in driving the formation of ferromagnetic order. For simplicity, Fig. 4(d) proposes a new efficient avenue for developing applicable spintronic devices. The proposed multi-site systems provide more opportunities to control novel quantum states. A critical issue is the production of flat bands, whether through Hund, Mott, or Kondo mechanisms.[30] Among these, Hund's coupling is likely the most important, and fortunately, it is intrinsic and widely present in itinerant correlated metals. The flat bands can enhance the DOS at the Fermi level, raising the possibility of forming the ferromagnetic order. Once the flat bands emerge and drive the magnetic phase transition, the resulting long-range magnetic order rapidly reduces spin fluctuations and promotes flat band formation through positive feedback. We recognize that more high- $T_C$  candidate spintronic devices could be discovered through this microscopic mechanism.

In summary, our magnetic DFT+DMFT calculations on  $\text{Fe}_3\text{GaTe}_2$  reveal a ferromagnetic phase transition occurring spontaneously above 300 K. This study not only confirms the crucial role of strongly correlated effects but also elucidates the microscopic mechanism underlying the formation of flat bands. For the first time, we explicitly propose a close relationship between flat bands and high- $T_C$  transition temperatures. Our findings provide a feasible and efficient approach to identifying more high- $T_C$  candidates for spintronic applications.

## Methods

**First-principles calculations.** First-principles DFT calculations were performed using the full-potential linearized augmented plane-wave (FLAPW) method, as implemented in the WIEN2k package.[42] The Perdew–Burke–Ernzerhof (PBE) functional was employed to represent the exchange-correlation potential.[43] To account for the strong correlation effects in transition metal elements, an effective Coulomb repulsion  $U_{\text{eff}}$  of 5.0 eV was applied to the Fe atoms in the GGA+U framework, utilizing the self-interaction correction method introduced by Anisimov.[44] To address the dynamical electronic correlations of Fe- $d$  orbitals, we performed DFT+DMFT calculations.[45] The hybridization expansion continuous-time quantum Monte Carlo (CT-HYB) method was used as the impurity solver.[46, 47] The correlation parameters were set to  $U = 5.5$  eV and  $J = 0.7$  eV. For the magnetic DFT+DMFT calculations, we considered 10 Fe- $d$  orbitals per Fe atoms and induced symmetry breaking by modifying the real part of the initial self-energy for both types of Fe atoms.

## Author contributions

Y. X. and F. T. conceived the idea and supervised the project; Y. X. and X. J. performed the calculations; X. J., J. X., and H. Z. participated in the discussions. Y. X. wrote the paper with input from all authors. All authors contributed to the interpretation of the data and revised the paper.

## Notes

The authors declare no competing financial interest.

## Acknowledgements

The authors thank Yue-Chao Wang, Yu Liu and Min Liu for the fruitful discussions. This work is supported by the National Natural Science Foundation of China (Grant Nos. 12204033, 52371174), the Fundamental Research Funds for the Central Universities (Grant No. FRF-TP-22-097A1), the State Key Lab of Advanced Metals and Materials (Grant No. 2022Z-13) and the Young Elite Scientist Sponsorship Program by BAST (Grant No. BYESS2023301). Numerical computations were performed on Hefei advanced computing center.

\* [yuanjixu@ustb.edu.cn](mailto:yuanjixu@ustb.edu.cn)

† [fuyang@ustb.edu.cn](mailto:fuyang@ustb.edu.cn)

- [1] Sarkar, D.; Xie, X. J.; Liu, W.; Cao, W.; Kang, J. H.; Gong, Y. J.; Kraemer, S.; Ajayan, P. M.; Banerjee, K. A subthermionic tunnel field-effect transistor with an atomically thin channel. *Nature* **2015**, 526 (7571), 91–95.
- [2] Sarkar, D.; Liu, W.; Xie, X. J.; Anselmo, A. C.; Mitragotri, S.; Banerjee, K.  $\text{MoS}_2$  field-effect transistor for next-generation label free biosensors. *ACS Nano* **2014**, 8 (4), 3992–4003.
- [3] Liu, C. S.; Chen, H. W.; Wang, S. Y.; Liu, Q.; Jiang, Y. G.; Zhang, D. W.; Liu, M.; Zhou, P. Two-dimensional materials for next-generation computing technologies. *Nat. Nanotechnol.* **2020**, 15 (7), 545–557.
- [4] Yang, H.; Valenzuela, S. O.; Chshiev, M.; Couet, S.; Dineny, B.; Dlubak, B.; Fert, A.; Garello, K.; Jamet, M.; Jeong, D.-E.; Lee, K.; Lee, T.; Martin, M.-B.; Kar, G. S.; S en eol, P.; Shin, H.-J.; Roche, S. Two-dimensional materials prospects for non-volatile spintronic memories. *Nature* **2022**, 606 (7915), 663–673.
- [5] Gong, C.; Zhang, X. Two-dimensional magnetic crystals and emergent heterostructure devices. *Science* **2019**, 363 (6428), eaav4450.
- [6] Kajale, S. N.; Hanna, J.; Jang, K.; Sarkar D. Two-dimensional magnetic materials for spintronic applications. *Nano Res.* **2024** 17 (2), 743–762.
- [7] Zhang, G.; Guo, F.; Wu, H.; Wen, X.; Yang, L.; Jin, W.; Zhang, W.; Chang, H. Above-room-temperature strong intrinsic ferromagnetism in 2D van der Waals  $\text{Fe}_3\text{GaTe}_2$  with large perpendicular magnetic anisotropy. *Nat. Commun.* **2022**, 13 (1), 5067.
- [8] Fei, Z.; Huang, B.; Malinowski, P.; Wang, W.; Song, T.; Sanchez, J.; Yao, W.; Xiao, D.; Zhu, X.; May, A. F.; Wu, W.; Cobden, D. H.; Chu, J. H.; Xu, X. Two-dimensional itinerant ferromagnetism in atomically thin  $\text{Fe}_3\text{GeTe}_2$ . *Nat. Mater.* **2018**, 17 (9), 778–782.
- [9] Deng, Y.; Yu, Y.; Song, Y.; Zhang, J.; Wang, N. Z.; Sun, Z.; Yi, Y.; Wu, Y. Z.; Wu, S.; Zhu, J.; Wang, J.; Chen, X. H.; Zhang, Y. Gate-tunable room-temperature ferromagnetism in two-dimensional  $\text{Fe}_3\text{GeTe}_2$ . *Nature* **2018**, 563 (7729), 94–99.
- [10] Ikeda, S.; Miura, K.; Yamamoto, H.; Mizunuma, K.; Gan, H. D.; Endo, M.; Kanai, S.; Hayakawa, J.; Matsukura, F.; Ohno, H. A perpendicular-anisotropy  $\text{CoFeB}$ – $\text{MgO}$  magnetic tunnel junction. *Nat. Mater.* **2010**, 9 (9), 721–724.
- [11] Gong, C.; Li, L.; Li, Z.; Ji, H.; Stern, A.; Xia, Y.; Cao, T.; Bao, W.; Wang, C.; Wang, Y.; Qiu, Z. Q.; Cava, R. J.; Louie, S. G.; Xia, J.; Zhang, X. Discovery of intrinsic ferromagnetism in two-dimensional van der Waals crystals. *Nature* **2017**, 546 (7657), 265–269.
- [12] Ruiz, A. M.; Esteras, D. L.; L opez-Alcal a, D.; Baldov ı, J. J. On the origin of the above-room-temperature magnetism in the 2D van der Waals ferromagnet  $\text{Fe}_3\text{GaTe}_2$ . *Nano Lett.* **2024**, 24 (26), 7886–7894.
- [13] Ghosh, S.; Ershadrad, S.; Borisov, V.; Sanyal, B. Unraveling effects of electron correlation in two-dimensional  $\text{Fe}_n\text{GeTe}_2$  ( $n = 3, 4, 5$ ) by dynamical mean field theory. *npj npj Comput. Mater.* **2023**, 9 (1), 1–16.
- [14] Lee, J.-E.; Yan, S.; Oh, S.; Hwang, J.; Denlinger, J. D.; Hwang, C.; Lei, H.; Mo, S. K.; Park, S. Y.; Ryu, H.

- Electronic structure of above-room-temperature van der Waals ferromagnet  $\text{Fe}_3\text{GaTe}_2$ . *Nano Lett.* **2023**, 23 (24), 11526-11532.
- [15] Ruiz, A. M.; Esteras, D. L.; López-Alcalá, D.; Baldoví, J. J. On the origin of the above-room-temperature magnetism in the 2D van der Waals ferromagnet  $\text{Fe}_3\text{GaTe}_2$ . *Nano Lett.* **2024**, 24 (26), 7886-7894.
- [16] Yin, Z. P.; Haule, K.; Kotliar, G. Kinetic frustration and the nature of the magnetic and paramagnetic states in iron pnictides and iron chalcogenides. *Nat. Mater.* **2011**, 10 (12), 932-935.
- [17] Georges, A.; Medici, L. d.; Mravlje, J. Strong correlations from Hund's coupling. *Annu. Rev. Condens. Matter Phys.* **2013**, 4 (1), 137-178.
- [18] Georges, A.; Kotliar, G. The Hund-metal path to strong electronic correlations. *Physics Today* **2024**, 77 (4), 46-53.
- [19] Bao, S.; Wang, W.; Shangguan, Y.; Cai, Z.; Dong, Z.-Y., Huang, Z.; Si, W.; Ma, Z.; Kajimoto, R.; Ikeuchi, K.; Yano, S.-i.; Yu, S.-L.; Wan, X.; Li, J.-X.; Wen, J. Neutron spectroscopy evidence on the dual nature of magnetic excitations in a van der Waals metallic ferromagnet  $\text{Fe}_{2.72}\text{GeTe}_2$ . *Phys. Rev. X* **2022**, 12 (1), No. 011022.
- [20] Zhu, J. X.; Janoschek, M.; Chaves, D. S.; Cezar, J. C.; Durakiewicz, T.; Ronning, F.; Sassa, Y.; Mansson, M.; Scott, B. L.; Wakeham, N.; Bauer, E. D.; Thompson, J. D. Electronic correlation and magnetism in the ferromagnetic metal  $\text{Fe}_3\text{GeTe}_2$ . *Phys. Rev. B* **2016**, 93 (14), No. 144404.
- [21] Zhang, Y.; Lu, H.; Zhu, X.; Tan, S.; Feng, W.; Liu, Q.; Zhang, W.; Chen, Q.; Liu, Y.; Luo, X.; Xie, D.; Luo, L.; Zhang, Z.; Lai, X. Emergence of Kondo lattice behavior in a van der Waals itinerant ferromagnet,  $\text{Fe}_3\text{GeTe}_2$ . *Sci. Adv.* **2018**, 4 (1), No. eaao6791.
- [22] Zhao, M.; Chen, B.-B.; Xi, Y.; Zhao, Y.; Xu, H.; Zhang, H.; Cheng, N.; Feng, H.; Zhuang, J.; Pan, F.; Xu, X.; Hao, W.; Li, W.; Zhou, S.; Dou, S. X.; Du, Y. Kondo holes in the two-dimensional itinerant Ising ferromagnet  $\text{Fe}_3\text{GeTe}_2$ . *Nano Lett.* **2021**, 21 (14), 6117-6123.
- [23] Corasaniti, M.; Yang, R.; Sen, K.; Willa, K.; Merz, M.; Haghghirad, A. A.; Le Tacon, M.; Degiorgi, L. Electronic correlations in the van der Waals ferromagnet  $\text{Fe}_3\text{GeTe}_2$  revealed by its charge dynamics. *Phys. Rev. B* **2020**, 102 (16), No. 161109(R).
- [24] Chen, B.; Yang, J.; Wang, H.; Imai, M.; Ohta, H.; Michioka, C.; Yoshimura, K.; Fang, M. Magnetic properties of layered itinerant electron ferromagnet  $\text{Fe}_3\text{GeTe}_2$ . *J. Phys. Soc. Jpn.* **2013**, 82 (12), No. 124711.
- [25] Xu, X.; Li, Y. W.; Duan, S. R.; Zhang, S. L.; Chen, Y. J.; Kang, L.; Liang, A. J.; Chen, C.; Xia, W.; Xu, Y.; Malinowski, P.; Xu, X. D.; Chu, J.-H.; Li, G.; Guo, Y. F.; Liu, Z. K.; Yang, L. X.; Chen, Y. L. Signature for non-Stoner ferromagnetism in the van der Waals ferromagnet  $\text{Fe}_3\text{GeTe}_2$ . *Phys. Rev. B* **2020**, 101 (20), No. 201104(R).
- [26] Wu, H.; Hu, C.; Xie, Y.; Jang, B. G.; Huang, J.; Guo, Y.; Wu, S.; Hu, C.; Yue, Z.; Shi, Y.; Basak, R.; Ren, Z.; Yilmaz, T.; Vescovo, E.; Jozwiak, C.; Bostwick, A.; Rotenberg, E.; Fedorov, A.; Denlinger, J. D.; Klewe, C.; Shafer, P.; Lu, D.; Hashimoto, M.; Kono, J.; Frano, A.; Birge-neau, R. J.; Xu, X.; Zhu, J.-X.; Dai, P.; Chu, J.-H.; Yi, M. Spectral evidence for local-moment ferromagnetism in the van der Waals metals  $\text{Fe}_3\text{GaTe}_2$  and  $\text{Fe}_3\text{GeTe}_2$ . *Phys. Rev. B* **2020**, 109 (10), No. 104410.
- [27] Xu, Y.; Wang, Y.; Jin, X.; Liu, H.; Liu, Y.; Song, H.; Tian, F. Mechanism of magnetic phase transition in correlated magnetic metal: insight into itinerant ferromagnet  $\text{Fe}_{3-\delta}\text{GeTe}_2$ . *arXiv (cond-mat.str-el)*, 6 Jul 2024, DOI: 10.48550/arXiv.2407.04957 (accessed 2024-07-06).
- [28] Rosa, P. F. S.; Ronning, F. A quantum collaboration for flat bands. *Nat. Phys.* **2024**, 20 (4), 539-540.
- [29] Huang, J.; Chen, L.; Huang, Y.; Setty, C.; Gao, B.; Shi, Y.; Liu, Z.; Zhang, Y.; Yilmaz, T.; Vescovo, E.; Hashimoto, M.; Lu, D.; Yakobson, B. I.; Dai, P.; Chu, J.-H.; Si, Q.; Yi, M. Non-Fermi liquid behaviour in a correlated flat-band pyrochlore lattice. *Nat. Phys.* **2024**, 20 (4), 603-609.
- [30] Checkelsky, J. G.; Bernevig, B. A.; Coleman, P.; Si, Q.; Paschen, S. Flat bands, strange metals and the Kondo effect. *Nat. Rev. Mater.* **2024**, 9 (7), 509-526.
- [31] Georges, A.; Kotliar, G.; Krauth, W.; Rozenberg, M. J.; Dynamical mean-field theory of strongly correlated fermion systems and the limit of infinite dimensions. *Rev. Mod. Phys.* **1996**, 68 (1), 13-125.
- [32] Kotliar, G.; Savrasov, S. Y.; Haule, K.; Oudovenko, V. S.; Parcollet, O.; Marianetti, C. A. Electronic structure calculations with dynamical mean-field theory. *Rev. Mod. Phys.* **2006**, 78 (3), 865-951.
- [33] Stoner, E. C. Ferromagnetism. *Rep. Prog. Phys.* **1947**, 11 (1), 43-112.
- [34] Kim, T. J.; Ryee, S.; Han, M. J.  $\text{Fe}_3\text{GeTe}_2$ : a site-differentiated Hund metal. *npj Comput. Mater.* **2022**, 8 (1), No. 245.
- [35] Bai, X.; Lechermann, F.; Liu, Y.; Cheng, Y.; Kolesnikov, A. I.; Ye, F.; Williams, T. J.; Chi, S.; Hong, T.; Granroth, G. E.; May, A. F.; Calder, S. Antiferromagnetic fluctuations and orbital-selective Mott transition in the van der Waals ferromagnet  $\text{Fe}_{3-x}\text{GeTe}_2$ . *Phys. Rev. B* **2022**, 106 (18), No. L180409.
- [36] Stewart, G. R. Heavy-fermion systems. *Rev. Mod. Phys.* **1984**, 56 (4), 755-787.
- [37] Yang, Y.-F.; Fisk, Z.; Lee, H. O.; Thompson, J. D.; Pines, D.; Scaling the Kondo lattice. *Nature* **2008**, 454 (7204), 611-613.
- [38] Shim, J. H.; Haule, K.; Kotliar, G.; Modeling the localized-to-itinerant electronic transition in the heavy fermion system  $\text{CeIrIn}_5$ . *Science* **2007**, 318 (5856), 1615-1617.
- [39] Xu, Y.; Sheng, Y.; Yang, Y. Mechanism of the insulator-to-metal transition and superconductivity in the spin liquid candidate  $\text{NaYbSe}_2$  under pressure. *npj Quantum Mater.* **2022**, 7 (1), No. 21.
- [40] Yu, T. L.; Xu, M.; Yang, W. T.; Song, Y. H.; Wen, C. H. P.; Yao, Q.; Lou, X.; Zhang, T.; Li, W.; Wei, X. Y.; Bao, J. K.; Cao, G. H.; Dudin, P.; Denlinger, J. D.; Strocov, V. N.; Peng, R.; Xu, H. C.; Feng, D. L. Strong band renormalization and emergent ferromagnetism induced by electron-antiferromagnetic-magnon coupling. *Nat. Commun.* **2022**, 13 (1), No. 6560.
- [41] Deng, X.; Stadler, K. M.; Haule, K.; Weichselbaum, A.; von Delft, J.; Kotliar, G. Signatures of Mottness and Hundness in archetypal correlated metals. *Nat. Commun.* **2019**, 10 (1), No. 2721.
- [42] Blaha, P.; Schwarz, K.; Madsen, G. K. H.; Kvasnicka, D.; Luitz, J.; Laskowski, R.; Tran, F.; Marks, L. D. *WIEN2k: An augmented plane wave plus local orbitals program for calculating crystal properties*; Vienna University of Technology, Austria, 2023.
- [43] Perdew, J. P.; Burke, K.; Ernzerhof, M. Generalized gra-

- dient approximation made simple. *Phys. Rev. Lett.* **1996**, 77 (18), 3865-3868.
- [44] Anisimov, V. I.; Solovyev, I. V.; Korotin, M. A.; Czyzyk, M. T.; Sawatzky, G. A. Density-functional theory and NiO Photoemission spectra. *Phys. Rev. B* **1993**, 48 (23), 16929-16934.
- [45] Haule, K.; Yee, C.-H.; Kim, K. Dynamical mean-field theory within the full-potential methods: electronic structure of CeIrIn<sub>5</sub>, CeCoIn<sub>5</sub>, and CeRhIn<sub>5</sub>. *Phys. Rev. B* **2010**, 81 (19), No. 195107.
- [46] Werner, P.; Comanac, A.; de' Medici, L.; Troyer, M.; Millis, A. J. Continuous-time solver for quantum impurity models. *Phys. Rev. Lett.* **2006**, 97 (7), No. 076405.
- [47] Haule, K. Quantum Monte Carlo impurity solver for cluster dynamical mean-field theory and electronic structure calculations with adjustable cluster base. *Phys. Rev. B* **2007**, 75 (15), No. 155113.